

Structural and Magnetic Properties of Mechanically Alloyed and Oxidized Fe-Based Powder Mixtures

S. Azzaza^{1,2} · F. Hedef^{2,3} · R. Chater⁴ · H. Abbas⁵ · N. Zerniz⁴ · A. Benmoussa⁴ · M. Bououdina^{6,7}

Received: 18 January 2016 / Accepted: 22 January 2016 / Published online: 12 February 2016
© Springer Science+Business Media New York 2016

Abstract Nanostructured $\text{Fe}_{1-x}\text{Ni}_x$ and $\text{Fe}_{1-x-y}\text{Ni}_x\text{Cr}_y$ ($x = 30, 40$; $y = 10$) powders were obtained by mechanical alloying technique (MA) from elemental powders using a planetary ball mill. The evolution of structure, microstructure and magnetic properties of mechanically alloyed powders were studied by X-ray diffraction, scanning electron microscopy and a vibrating sample magnetometer. The MA powders for 7 h consist of two solid solutions bcc and fcc. The saturation magnetization was found to decrease with

increasing Ni content and so with increasing fcc solid solution amount. Oxidation of MA powders results in the formation of three phases: antiferromagnetic NiO, hematite $\alpha\text{-Fe}_2\text{O}_3$, and ferrimagnetic spinel structure NiFe_2O_4 . According to the magnetic measurements, the oxidation leads to the deterioration of magnetic behavior due to the exchange bias anisotropy.

Keywords Fe-Ni-Cr alloys · Mechanical alloying · Oxidation · Magnetization

✉ F. Hedef
hedef77@yahoo.fr

¹ Laboratory of Magnetism and Spectroscopy of Solids, Department of Physics, University Badji Mokhtar of Annaba, BP: 12, Annaba, 23000 Algeria

² Department of Technology, Faculty of Technology, University 20 Août 1955-Skikda, BP 26, 21000 Skikda, Algeria

³ LRPCSI, Faculty of Sciences, University 20 Août 1955-Skikda, BP 26, 21000 Skikda, Algeria

⁴ Laboratory of Inorganic Materials Chemistry, Chemistry Department, University Badji Mokhtar of Annaba, BP: 12, Annaba, 23000 Algeria

⁵ Department of Biology, College of Science, University of Bahrain, PO Box 32038, Zallaq, Kingdom of Bahrain

⁶ Nanotechnology Centre, University of Bahrain, PO Box 32038, Zallaq, Kingdom of Bahrain

⁷ Department of Physics, College of Science, University of Bahrain, PO Box 32038, Zallaq, Kingdom of Bahrain

1 Introduction

The research of nanocrystalline magnetic materials has known a huge development in the last decades. This is due to the properties common to both nanostructured amorphous and crystalline materials and their ability to compete with their bulk counterparts. The benefits found in the nanocrystalline alloys stem from their chemical and structural changes at the nanoscale due to quantum confinement effects, which are important for developing optimal magnetic properties [1–3].

Fe-Ni alloys have long been known, and they are widely applied to magnetic components in electric power industry, such as transformer magnets and magnetic cores, because of their excellent soft magnetic properties of low coercivity and high saturation magnetization. Several methods were used for the development of FeNi-based nanomaterials, including thermal evaporation [4], electro deposition [5], gas condensation [6], rapid solidification [7], metal plasma reaction [8], and mechanical alloying (MA) [9–11].

In MA, it is well established that magnetic properties can be improved by adjusting the composition and morphology

of the alloy powders. Also this purpose can be achieved by introducing other elements thus leading to ternary or quaternary alloys [12]. Fe-Ni-Cr alloys are widely used in many areas due to their good corrosion resistance, magnetoresistive, and mechanical properties [13–15]. Fe–Cr–Ni ternary system has also been recognized as one fundamental importance for solid oxide fuel cell applications [16]. It has been reported that most of the preparation ways of Fe-Ni-Cr alloys are melting. However, due to the ductility and the high strength of Ni and Cr, it is so difficult to break the refinement and to get the nanocrystalline flake powder which has a super soft ferromagnetic character [12]. Recent works on MA Fe–Ni–Cr have been done by Refs. [12, 17, 18]; however, to our knowledge, no reports on the oxidation behavior of Fe-Ni-Cr alloys obtained by mechanical alloying have been found in the literature.

The synthesis of $\text{Fe}_{70}\text{Ni}_{30}$, $\text{Fe}_{60}\text{Ni}_{40}$, $\text{Fe}_{60}\text{Ni}_{30}\text{Cr}_{10}$, and $\text{Fe}_{50}\text{Ni}_{40}\text{Cr}_{10}$ alloy compositions from elemental powders by mechanical alloying is reported in this paper. The aim of the present work is to study the processing of Fe–Ni and Fe-Ni-Cr soft magnetic materials by the MA technique. The effect of the oxidation on structural and microstructural

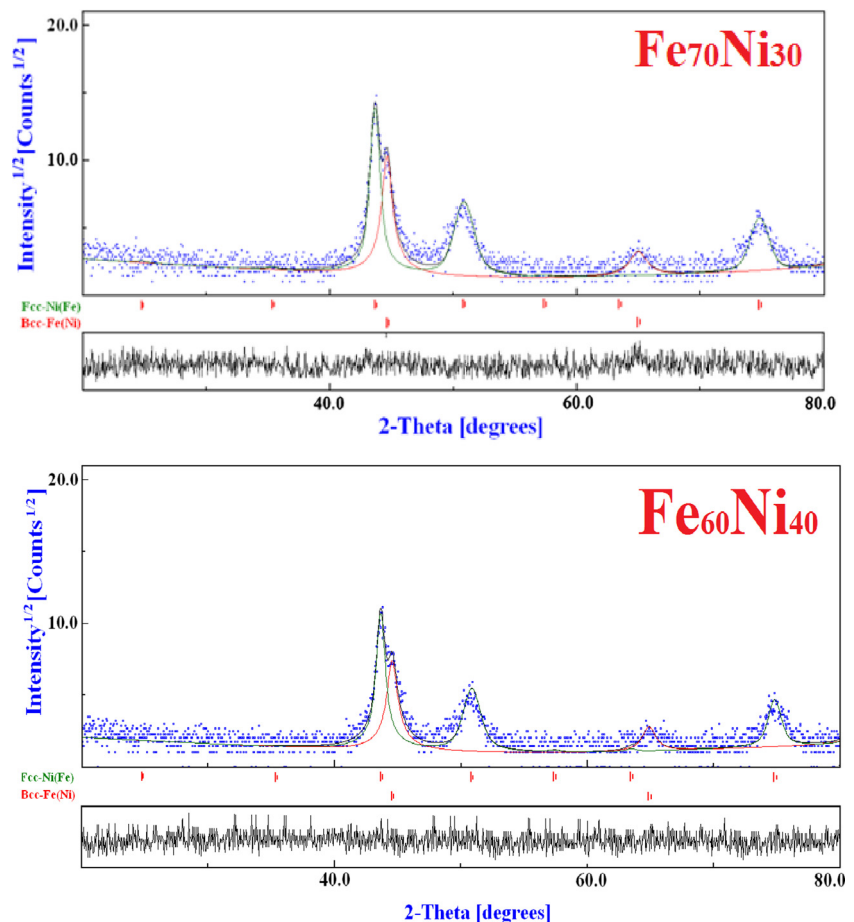
evolution and thereby magnetic properties' modifications was also investigated.

2 Experimental Details

2.1 Preparation of Samples

All grinding experiments of $\text{Fe}_{1-x}\text{Ni}_x$ and $\text{Fe}_{1-x-y}\text{Ni}_x\text{Cr}_y$ powder mixtures were conducted using a high-energy Planetary Ball Mill (Fritsch P7). The reagents, iron (Fe, 99.9 %), nickel (Ni, 99.9 %), and chromium (Cr, 99.9 %); powders; as well as stainless steel balls are introduced in a stainless steel bowl of 60 ml, under inert atmosphere inside a glove box with purified argon circulation. The lid fitted with a gasket is screwed on the cylindrical body of the bowl, which is then placed in the mill. The grindings were realized at room temperature. The milling conditions used are 3 g of powder mixtures, six balls of 12-mm diameter (giving a ball-to-powder weight ratio of 25:1), 7 h of milling period, and a speed of 300 rpm. The milling was carried out by cycles of 30 min followed by 15 min of pause. The bowls are

Fig. 1 Rietveld refinement of the XRD pattern of the MA $\text{Fe}_{70}\text{Ni}_{30}$ ($R_{\text{wp}} = 7.02\%$, $\text{Gof} = 1.41$) and $\text{Fe}_{60}\text{Ni}_{40}$ ($R_{\text{wp}} = 5.87\%$, $\text{Gof} = 1.39$) powders under air. Experimental (blue line) and calculated (black line) patterns are shown. The difference is given



open only after a period of cooling of 30 up to 60 min. The milling of powder mixtures led to products of black colour and clearly of crystalline nature.

2.2 Oxidation of Milled Powders

High-temperature oxidation of the milled Fe-Ni and Fe-Ni-Cr powder mixtures was performed at a fixed temperature of 1000 °C. The samples were placed in a platinum crucible once the oxidation temperature is reached; the whole system (platinum crucible containing the powder) is placed in a furnace (Nabertherm) programmable resistance. The actual oxidation was programmed under ambient air at atmospheric pressure. The oxidation was carried for a period of 24 h; after the oxidation is completed, the furnace is cooled down to room temperature under air.

2.3 Characterization Techniques

The characterization of powders was followed by X-ray diffraction (XRD) using Rigaku diffractometer Ultima IV equipped with Cu-K α radiation ($\lambda_{Cu} = 0.15406$ nm) in a (θ -2 θ) Bragg-Brentano geometry. Microstructure analysis and morphology observations were carried out using ZEISS EVO LS 10 electron microscope (SEM) operating at an

acceleration voltage of 20 KV equipped with an electron-dispersive spectrometer (EDS) Bruker 127 eV detector for chemical composition. Magnetic measurements were performed at room temperature by means of PMC MicroMag 3900 model vibrating sample magnetometer (VSM) having a 1-Tesla magnet.

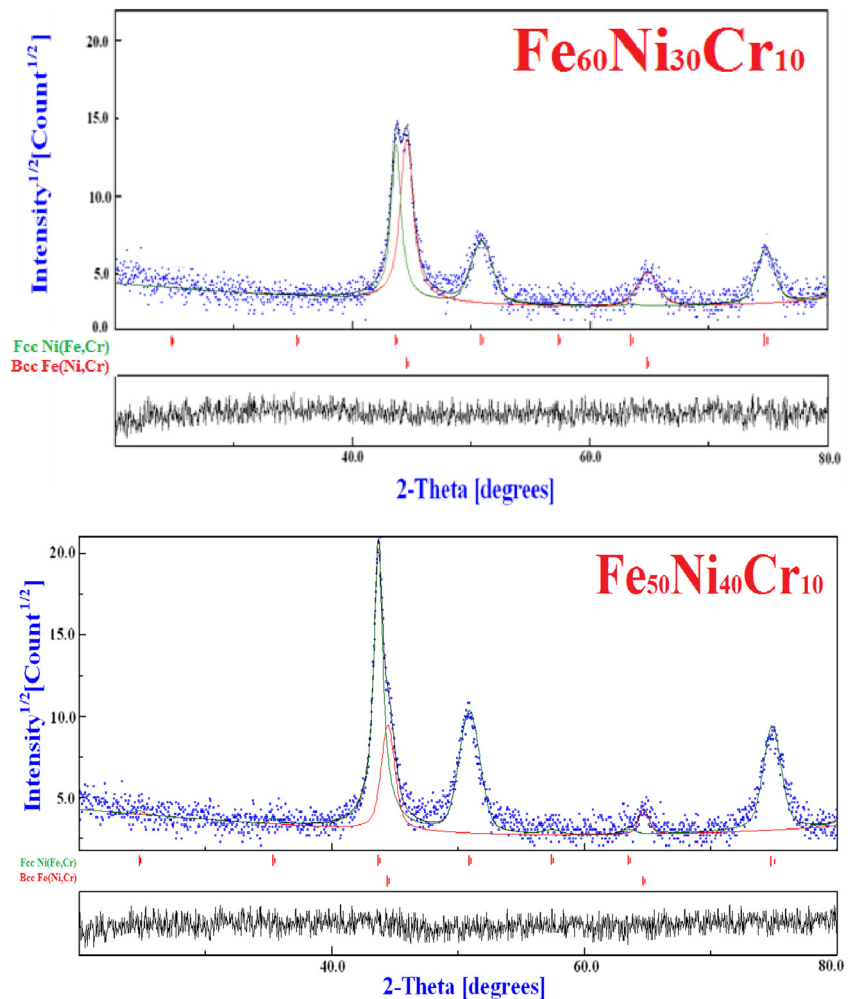
2.4 Qualitative and Quantitative Phase Analysis

Since X-ray diffraction powder patterns of the samples are composed of a large number of overlapping reflections, the Rietveld’s analysis based on structure and microstructure refinements [19, 20] has been adopted for precise determination of several structural and microstructural parameters. In this method, the background and peak profiles for all phases present in the sample are evaluated. Background is usually described by a polynomial function. For each reflection, the profile is defined by the angular position, the intensity, and the peak shape. The position and the intensity are evaluated from the crystal structure and phase composition. The methodology includes residual stresses, texture, and microstructure contributions, i.e., crystallite size, microstrain, and defect concentrations. Indeed, the stress field modifies the peak positions and the texture of the sample affects the integrated intensities of the reflections and the microstructure changes of the peak shape profile.

Table 1 Microstructural parameters of MA and oxidized Fe-Ni and Fe-Ni-Cr powders

Compositions	MA for 7 h					MA for 7 h + oxidation					
	Phases	$a/\text{\AA}$ ($\pm 2 \times 10^{-4}$)	$\langle d \rangle / \text{nm}$ (± 2)	$\langle \sigma^2 \rangle$ ($1/2\%$) ($\pm 10^{-3}$)	Amount/% (± 0.2)	Phases	$a/\text{\AA}$ ($\pm 10^{-3}$)	$c/\text{\AA}$ ($\pm 10^{-3}$)	$\langle d \rangle / \text{nm}$ (± 1)	$\langle \sigma^2 \rangle$ ($1/2\%$) ($\pm 10^{-3}$)	Amount/% (± 0.2)
Fe70Ni30	Bcc Fe(Ni)	2.870	14.435	0.073	28.413	Fe2O3	5.034	13.742	69	0.053	26.1
	Bcc Fe(Ni)	2.870	21.461	0.281	71.587	NiFe2O4	8.338	–	69	0.029	55.1
						NiO	4.175	–	38	0.067	14.8
						Bcc Fe	2.877	–	43	0.250	4.0
Fe60Ni40	Bcc Fe(Ni)	2.873	15.950	0.091	35.416	Fe2O3	5.035	13.738	71	0.029	22.7
	Fcc Ni(Fe)	3.588	19.248	0.397	64.584	NiFe2O4	5.035	–	67	0.111	58.3
						NiO	4.377	–	46	0.030	08.9
Fe60Ni30Cr10	Bcc Fe(Ni, Cr)	2.873	12.06	0.482	41.428	Fe2O3	5.035	13.738	52	0.081	18.5
	Fcc Ni(Fe, Cr)	3.587	13.66	0.876	58.572	NiFe2O4	8.337	–	77	0.237	56.5
						NiO	4.179	–	33	0.030	17.1
						NiO	2.882	–	69	0.260	8.0
						Fe(Ni,Cr)	5.034	13.743	36	0.120	5.2
Fe50Ni40Cr10	Bcc Fe(Ni, Cr)	2.882	21.29	0.291	33.294	Fe2O3	8.339	–	83	0.199	76.5
	Fcc Ni(Fe, Cr)	3.587	22.34	0.995	66.706	NiFe2O4	4.176	–	68	0.114	16.6
						NiO	3.527	–	34	0.100	1.7
						Fcc					
						Ni(Fe,Cr)					

Fig. 2 Rietveld refinements of the XRD pattern of the MA $\text{Fe}_{60}\text{Ni}_{30}\text{Cr}_{10}$ ($R_{\text{wp}} = 6.17\%$, $\text{GoF} = 1.14$) and $\text{Fe}_{50}\text{Ni}_{40}\text{Cr}_{10}$ ($R_{\text{wp}} = 5.65\%$, $\text{GoF} = 1.17$) powders under air. Experimental (blue line) and calculated (black line) patterns are shown. The difference is given



The Marquardt least-squares procedure was adopted for minimizing the difference between the observed and simulated powder diffraction patterns, and the minimization was carried out by using the reliability index parameter, R_{wp} (weighted residual error), R_{B} (Bragg factor), and R_{exp} (expected error). This leads to the value of goodness of fit, GoF [20, 21]:

$$\text{GoF} = R_{\text{wp}}/R_{\text{exp}} \quad (1)$$

Refinements continue until convergence is reached with the value of the quality factor, GoF, approaching 1.

To simulate the theoretical X-ray powder patterns, the following considerations were made:

- (i) For bcc Fe(Ni) and Fe(Ni, Cr) solid solutions, W-type structure (A2), space group Im-3m with Wyckoff position 2a.
- (ii) For fcc Ni(Fe) and Ni(Fe,Cr) solid solutions, type of structure (A1), the space group was taken as Fm-3m with Wyckoff position 2a.

- (iii) For NiO (cubic), the space group was taken as Fm-3m with Ni and O atoms in special Wyckoff positions 4(a) and 4(b), respectively.
- (iv) For $\alpha\text{-Fe}_2\text{O}_3$ (rhombohedral), the space group was taken as R3-c, with Fe and O atoms in special Wyckoff positions 12(c) and 18(e), respectively.
- (v) For NiFe_2O_4 (cubic, normal spinel), the space group was taken as Fd3-m with Ni, Fe, and O atoms in the special Wyckoff positions 8(f), 16(c), and 32(b), respectively.

3 Results and Discussion

3.1 Structure Analysis

The induced heavy plastic deformation into powder particles occurring during the milling process gives rise to the creation of a great amount of crystal defects such as dislocations, vacancies, interstitials, and grain boundaries

which promote solid-state reaction at ambient temperature. Depending on the initial mixture, changes in structure of mechanically alloyed powders can occur as follows: grain refinement, solid solution diffusion, and/or formation of new phases.

It was found that after 7 h of milling, all powders were completely synthesized. The best Rietveld refinement of the XRD patterns for the ball-milled $\text{Fe}_{70}\text{Ni}_{30}$ and $\text{Fe}_{60}\text{Ni}_{40}$ powder mixtures reveals the co-existence of two solid solutions: bcc α -Fe(Ni) and fcc γ -Ni(Fe) (Fig. 1). Since the nickel and iron form substantial solid solutions over the complete range of compositions, the formation of α and γ solid solutions indicates that a part of Ni atoms dissolved into bcc-Fe crystal lattice to form α -Fe(Ni); meanwhile, part of Fe atoms dissolve into fcc-Ni crystal lattice to form γ -Ni(Fe). Since the diffusion coefficient of α -Fe is greater than that of Ni [22], thereby Fe atoms will diffuse into Ni faster than they are replaced by Ni atoms diffusing in the opposite direction [23]. This is why the proportion of γ -Ni(Fe) is higher than that of α -Fe(Ni) (Table 1). The

observation of two structures bcc and fcc at room temperature is in good agreement with some results reported in the literature [22–24].

For $\text{Fe}_{60}\text{Ni}_{30}\text{Cr}_{10}$ and $\text{Fe}_{50}\text{Ni}_{40}\text{Cr}_{10}$ powder mixtures, the mechanical alloying leads to the formation of α -Fe and γ -Ni solid solutions due to (i) the diffusion of Cr and/or Ni into Fe crystal lattice and (ii) Fe and/or Cr into Ni crystal lattice, respectively (Fig. 2). However, Enayati et al. [17] reported only the formation of a nanostructured single-phase bcc solid solution (α) in mechanically alloyed Fe–18Cr–8Ni and Fe–15Cr–15Ni powders.

According to the thermodynamic data, Fe and Cr elements are insoluble at room temperature adding to the small heat of the mixing of Fe–Cr ($\Delta H_{\text{mix}} = -1$ kJ/mol atoms); the diffusion of Cr into Fe crystal lattice suggests that the local temperature increases during milling may also be responsible for solid-state reactions. Indeed, it was argued that the large plastic deformations that take place during the mechanical alloying process induce local melting at an atomic scale leading to the formation of new alloys [25].

From Table 1, one can see that the crystallite sizes decrease after 7 h of milling to 12.06 and 13.66 nm for bcc Fe(Ni, Cr) and fcc Ni(Fe, Cr) phases, respectively. This later is similar to that reported by Hadeif et al. [26] in MA $\text{Fe}_{50}\text{Ni}_{40}\text{Al}_{10}$ powders. On the other hand, the crystallite sizes of fcc phases are higher than those corresponding to bcc ones. Valderruten et al. [27] have shown in milled FeNi powders, where the fcc and bcc phases coexisted, that the crystallite size of the fcc phase was always greater than that of the bcc one. This difference is attributed to the fragile and ductile character of bcc and fcc phases, respectively.

The oxidation of mechanically alloyed powder mixtures leads to the formation of new phases due to the reaction of elemental powders with oxygen present in air. Hence, in addition to bcc-Fe (or fcc-Ni) solid solutions, all the XRD patterns show the presence of three oxides: NiO, α - Fe_2O_3 , and NiFe_2O_4 phases (Fig. 3). From the Rietveld refinement results, it is observed that the lattice parameter of NiFe_2O_4 structure increases with increasing Ni content and is slowly higher to that of pure crystalline NiFe_2O_4 ($a = 8.339$ Å; ICDD PDF #44-1485). The difference may be due to (i) the partial substitution of Fe^{3+} (0.55 Å) by Cr^{3+} (0.62 Å) since the preference of Cr^{3+} for octahedral environment is due to the favorable fit of the charge distribution of this ion in the crystal field at an octahedral site [28] and/or (ii) the redistribution of cations among the tetrahedral and octahedral interstices [29]. It was reported that if some of the oxygen vacancies (ionic radius of $\text{O}^{2-} = 1.38$ Å) are filled by the smaller Ni^{2+} ions (ionic radius = 0.78 Å) from tetrahedral sites, the ferrite lattice may show contraction during milling [30]. It has been reported that the ball-milled NiO

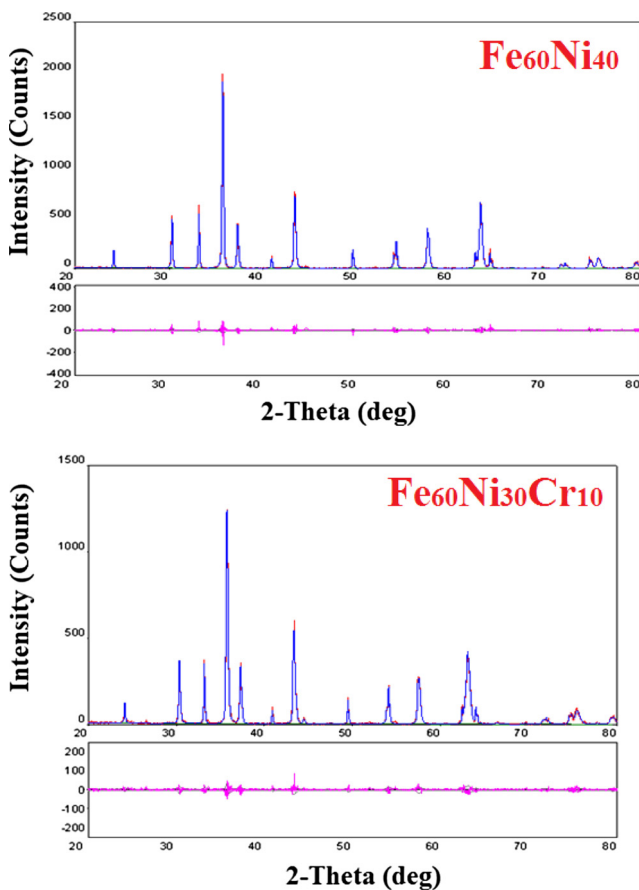


Fig. 3 Rietveld refinement of the XRD pattern of oxidized $\text{Fe}_{60}\text{Ni}_{40}$ ($R_{\text{wp}} = 18.41$ %, $\text{Gof} = 1.159$) and $\text{Fe}_{60}\text{Ni}_{30}\text{Cr}_{10}$ ($R_{\text{wp}} = 19.48$ %, $\text{Gof} = 1.169$) powders. Experimental (blue line) and calculated (pink line) patterns are shown. The difference is given

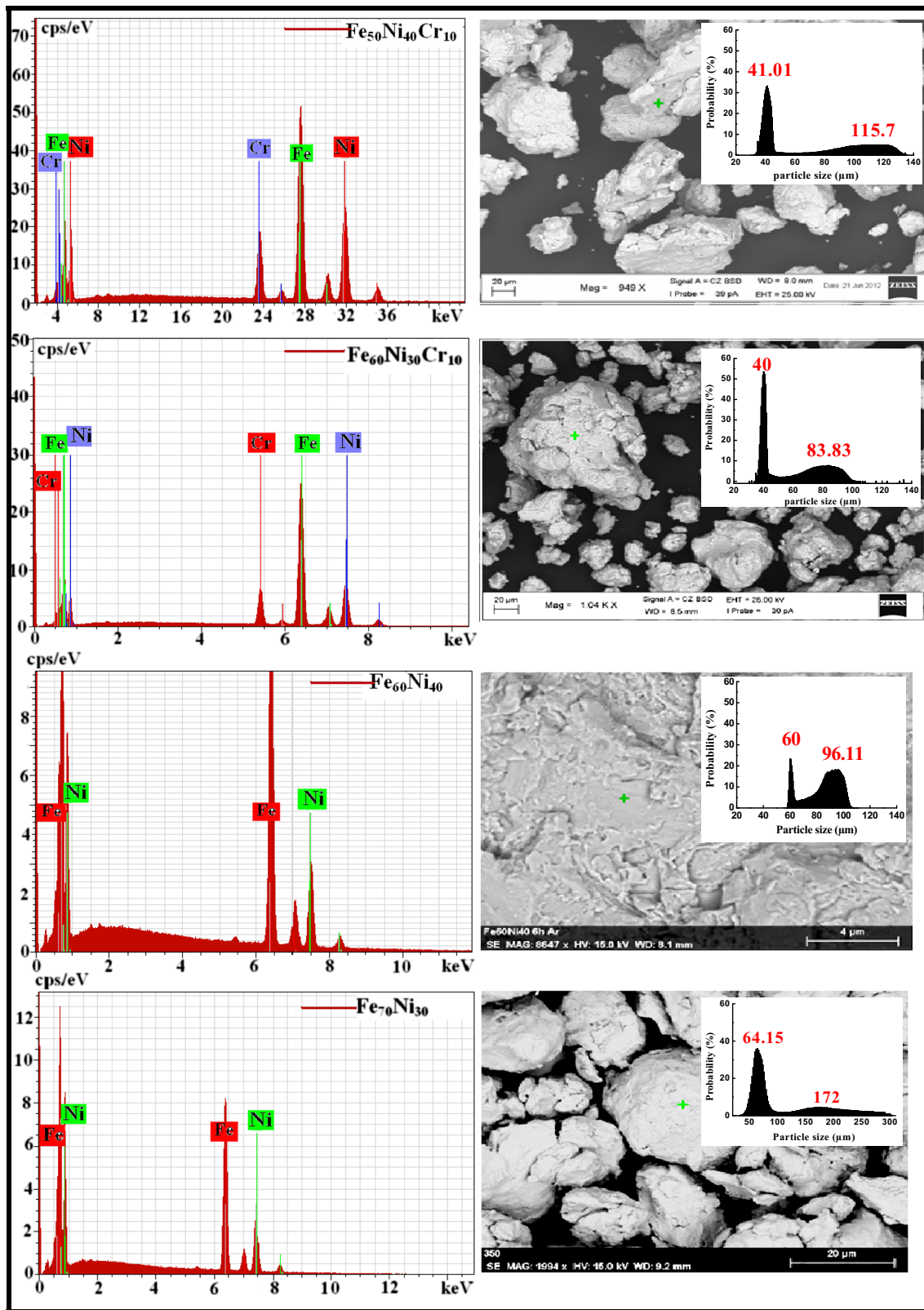


Fig. 4 SEM micrographs and EDS spectrum for MA Fe-Ni and Fe-Ni-Cr powder mixtures for 7 h

Table 2 Evolution of chemical composition of MA Fe-Ni and Fe-Ni-Cr powder mixtures

Compositions	Elements	Theoretical/ wt. %	Experimental analysis/wt. %	Error/%
Fe ₆₀ Ni ₄₀	Fe	60	63.34	1.6
	Ni	40	36.66	1.0
Fe ₇₀ Ni ₃₀	Fe	70	68.86	1.8
	Ni	30	31.14	0.8
Fe ₅₀ Ni ₄₀ Cr ₁₀	Fe	50	49.68	1.3
	Ni	40	40.07	1.0
	Cr	10	10.26	0.3
Fe ₆₀ Ni ₃₀ Cr ₁₀	Fe	60	60.92	1.5
	Ni	30	29.79	0.8
	Cr	10	09.29	0.3

and Fe₂O₃ powder mixtures in P5 ball mill lead to the formation of spinel structure NiFe₂O₄ after 1 h of milling with a lattice parameter of about 8.375 Å [31].

3.2 Microstructural Observations

Mechanical alloying causes drastic changes in the morphology of the powders that undergo severe plastic deformation. The SEM micrographs of FeNi and FeNiCr powders after 7 h of milling show different morphologies and distribution of particle sizes (Fig. 4). Due to the collision of the balls, the ductile powders are flattened by the compressive forces and hence the increase of surface area for contact leads to intimate contact between both flattened and un-flattened layers of particles. The severe deformation and work hardening lead to the disintegration of the agglomerated powders into fragments, giving rise to a bimodal distribution of particles size (see inset in Fig. 4). As an example, Fe₇₀Ni₃₀ powders show a lower bound average particle size of 64 μm and an upper bound average of 172 μm. The qualitative analysis, by EDS spectroscopy, shows the presence of the two elements Fe and Ni in MA Fe-Ni samples or three elements Fe, Ni, and Cr in MA Fe-Ni-Cr ones (Fig. 4). After 7 h of milling, the chemical composition varies slightly, almost close to the nominal composition of the samples as reported in Fig. 4 and Table 2.

SEM micrographs of the oxidized samples reveal the traces of oxide on the surface of particles (Fig. 5). This is expected as the powder particles are prone to oxidation and since high energy is imparted to the particles during milling, and the surface area increases which causes faster reaction with the environment at high temperature. Elemental analysis of the oxidized powders was performed by X-ray

energy-dispersive spectroscopy (EDS). The measurements were performed on several zones of the powders. The analysis of EDS spectra shows the presence of Fe, Ni, Cr, and O elements where the dominant element is oxygen. Table 3 shows the chemical composition (at.%) of the elements as identified by EDS analysis of samples oxidized for 24 h at 1000 °C in ambient air at atmospheric pressure. SEM and EDS analyses reveal the presence of three different zones: (i) zone 1 shows the presence of O and Fe, the ratio of oxygen and iron is around 3 to 2, which suggests the presence of Fe₂O₃ phase; (ii) zone 2 consists essentially of the spinel phase NiFe₂O₄, the Ni/Fe/O ratio in this zone being 1/2/4; and (iii) zone 3 showing the presence of Ni and O with a 1/1 ratio which suggests the presence of NiO phase. These results are in good agreement and confirm the results obtained by X-ray Rietveld analysis. For FeNiCr samples, similarly, EDS analysis reveals the presence of three zones; the presence of oxygen is likely to form Fe₂O₃, NiFe₂O₄, and NiO oxides. No Cr oxides have been observed.

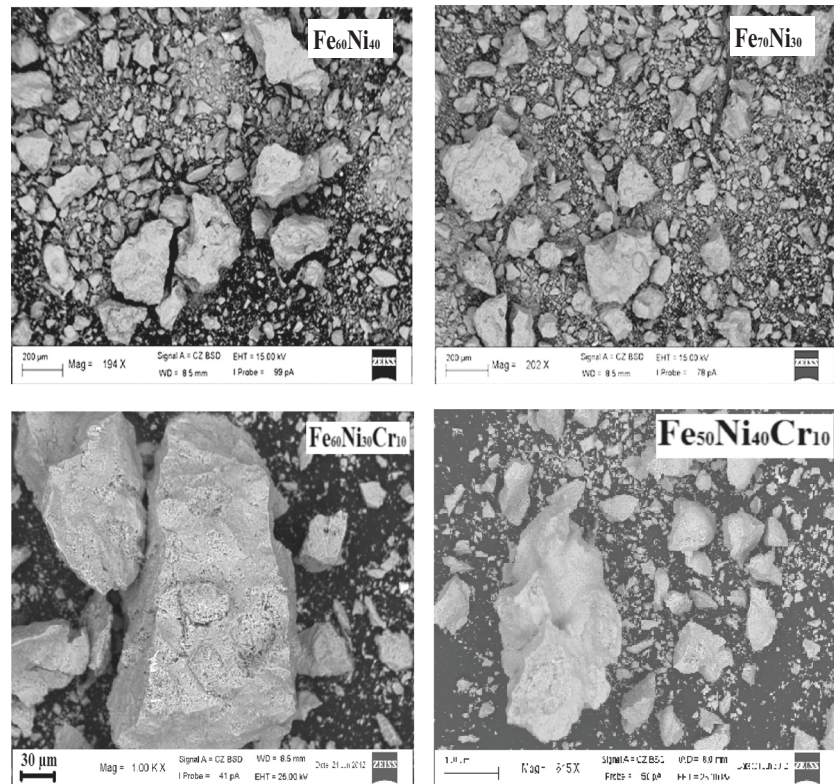
3.3 Magnetic Properties

A simultaneous occurrence of fcc and bcc phases, between 22.5 and 40 at.% Ni, was reported for milled Fe-Ni alloys, where the bcc phase shows a ferromagnetic character in contrast to the fcc phase which exhibits both the paramagnetic and ferromagnetic behaviors [32, 33]. Men'shikov et al. [34] had established qualitatively the ternary magnetic phase diagram of the Fe-Ni-Cr system through bulk magnetization and small-angle neutron scattering experiments. A.K. Majumdar et al. [35] studied the magnetic phase diagram of Fe_{80-x}Ni_xCr (10 ≤ x ≤ 30) and found that the system went through a compositional phase transition from long-range antiferromagnetic phase to a long-range ferromagnetic phase with a higher x value [18].

The saturation magnetization is generally regarded as independent of the microstructure and strongly depends on the chemical composition. Unlike the H_c, M_s is structurally insensitive. Remanence (M_r) is another magnetic property that also depends on the evolution of the microstructure of the sample. M_r is an indicative parameter of the amount of magnetization that the alloy or material is capable to store after a magnetic field was applied and withdrawn. The squareness ratio is given by the ratio of (M_r/M_s) and is essentially a measure of how square is the hysteresis loop (M-H) and is related to the level of intergrain interactions; it is seen to increase as the grain size decreases [36, 37].

Magnetic hysteresis (M-H) loops at room temperature of as-milled and oxidized powders are shown in Fig. 6. It can be seen that the sigmoidal hysteresis loops were narrow,

Fig. 5 SEM micrographs of the oxidized Fe-Ni and Fe-Ni-Cr powder mixtures



with a typical geometry of soft magnetic alloy hysteresis. After oxidation, the hysteresis loop becomes flattened. The values of M_s , H_c , M_r , and squareness ratio (M_r/M_s) obtained from loops are given in Table 4.

For MA powders, the M_s values are significantly lower than that of pure iron (220 emu/g). This may be attributed to the introduction of structural defects as well as microstrain in the sample during the milling process. Such defects cause volume expansion and consequently changes in geometry of the atomic arrangement and interatomic distances which have an effect on the exchange interaction and hence the mode of spin alignment. Since the magnetization is created by domain wall movement and spin rotation, it can thus be affected by the induced structural defects which serve as a pinning center for the domain wall motion. Furthermore, M_s is found to decrease with increasing Ni content and consequently to the increase of fcc phase amount [38]. It has been reported that the MA FeNi alloys with 22–28 % Ni are paramagnetic at room temperature due to the increase of fcc phase concentration [39]. On the other hand, it has long been known that in the fcc phase of Fe-Ni alloys, the Fe-Fe magnetic coupling could be antiferromagnetic for small Fe-Fe nearest-neighbor distance [40].

Hamzaoui et al. [41] have reported in binary Fe-Ni alloys a high magnetization saturation, and is close to $M_s = 227$ (Am^2/kg), and $M_s = 219$ (Am^2/kg), for MA Fe-10 %Ni and Fe-20 % Ni powders, respectively. A value of $M_s = 189$

(Am^2/kg) for (Fe–10 % Ni) 4 % Mo has been reported in ternary Fe-Ni-Mo alloys [42]. These values are much higher than those reported in this investigation.

The oxidation of milled powders leads to the (i) shift of loops to negative fields, (ii) increase of H_c , and (iii) decrease of M_s . The shift in hysteresis loop is expected when the field is applied in the reverse direction due to the presence of exchange anisotropy [43, 44] irrespective of the fact that the powder contains antiferromagnetic (or paramagnetic) phases. This shows that the oxide particles are separated from the ferromagnetic particles (FM) and may be in the form of a core shell structure as it is observed in SEM micrographs. The increase of H_c may arise because of the surface random anisotropy induced due to the presence of an antiferromagnetic oxide (AFM) in it. So the magnetic coupling of FM nanoparticles with AFM oxides provides a source of an effective additional anisotropy. The saturation magnetization is reduced from that of MA powders which can be explained by the presence of AFM oxide (NiO and $\alpha\text{-Fe}_2\text{O}_3$) as is evident from structural analysis. On the other hand, since the NiFe_2O_4 ferrimagnetic phase is dominant after oxidation (>50 %), the obtained values of M_s can be thus compared to that measured for the multidomain bulk NiFe_2O_4 (55 emu/g) [45]. Additionally, the lower value of M_s may be explained in terms of the core shell morphology of the nanoparticles consisting of ferrimagnetically aligned core spins and spin-glass-like surface layer.

Table 3 Evolution of chemical composition of MA Fe-Ni and Fe-Ni-Cr powder mixtures milled for 7 h and oxidized at 1000 °C

Compositions	Elements	Zone 1		Zone 2		Zone 3	
		Atom %	Error %	Atom %	Error %	Atom %	Error %
Fe ₆₀ Ni ₄₀	Fe	38.31	1.7	26.68	1.1	09.36	0.4
	Ni	00.47	0.0	12.69	0.6	38.95	1.6
	O	61.23	3.2	60.62	3.1	51.69	0.4
Fe ₇₀ Ni ₃₀	Fe	40.91	2.1	14.94	0.6	04.34	0.2
	Ni	00.28	0.0	30.01	1.3	51.18	2.3
	O	58.81	3.1	55.80	2.8	44.48	1.9
Fe ₅₀ Ni ₄₀ Cr ₁₀	Fe	55.35	2.0	38.35	1.4	03.64	0.2
	Ni	05.98	0.2	15.50	0.6	39.31	1.5
	Cr	01.78	0.1	01.03	0.1	07.34	0.3
	O	37.27	1.7	45.12	2.1	49.71	2.2
Fe ₆₀ Ni ₃₀ Cr ₁₀	Fe	22.94	1.1	22.32	1.1	04.87	0.2
	Ni	09.82	0.5	12.35	0.6	39.58	1.6
	Cr	07.75	0.4	07.02	0.3	07.88	0.3
	O	59.50	3.5	58.31	3.1	47.87	2.4

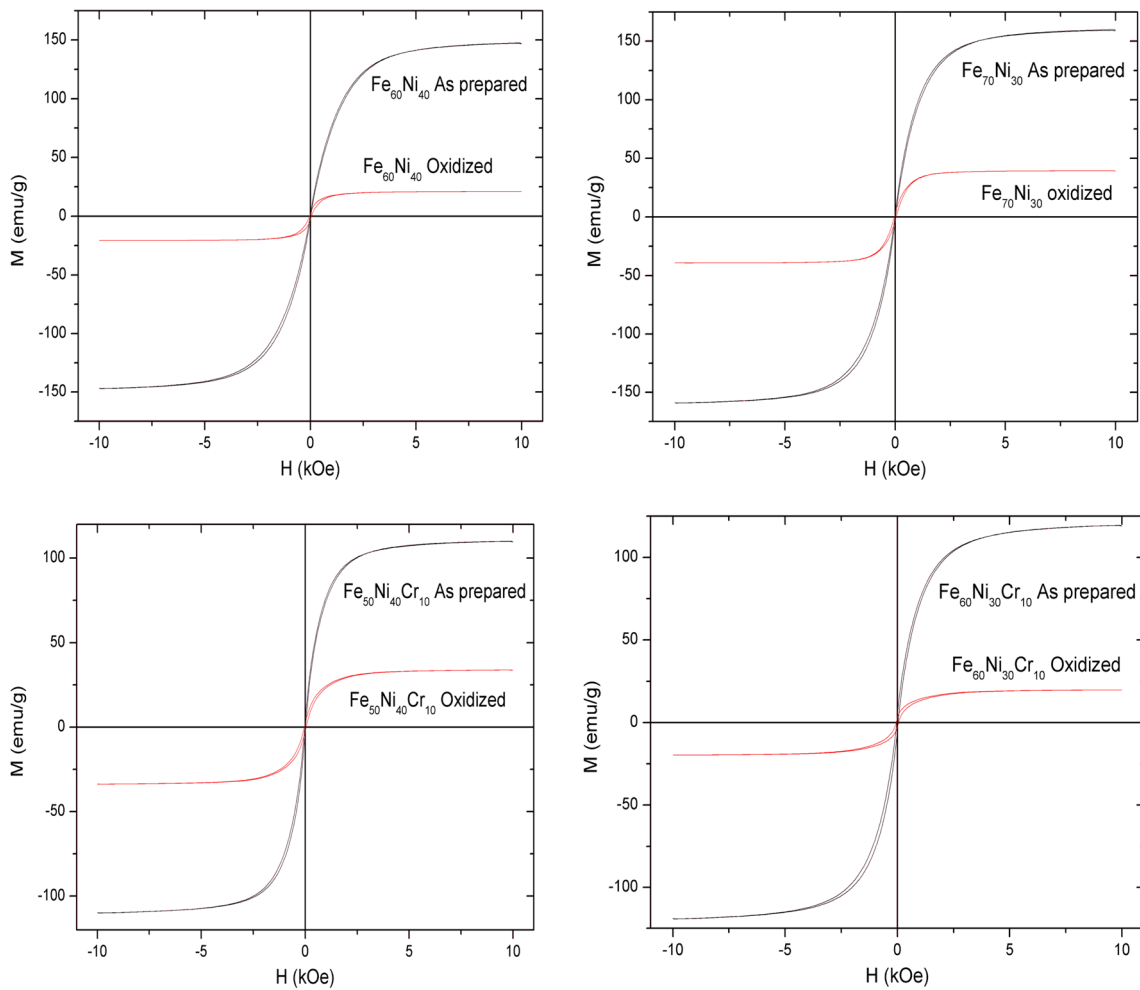


Fig. 6 Hysteresis loops of MA Fe-Ni and Fe-Ni-Cr powder mixtures

Table 4 Magnetic data of MA and oxidized Fe-Ni and Fe-Ni-Cr powders

Compositions	MA for 7 h				MA for 7 h + oxidation			
	Hc/Oe	Ms/emu/g	Mr/emu/g	Mr/Ms	Hc/Oe	Ms/emu/g	Mr/emu/g	Mr/Ms
Fe ₇₀ Ni ₃₀	15.45	159.1	2.44	0.015	43.11	39.27	3.05	0.08
Fe ₆₀ Ni ₄₀	15.28	147.0	1.77	0.01	47.36	20.96	2.55	0.12
Fe ₆₀ Ni ₃₀ Cr ₁₀	29.92	119.2	4.51	0.04	51.13	19.71	2.83	0.14
Fe ₅₀ Ni ₄₀ Cr ₁₀	17.13	109.8	2.60	0.02	44.94	33.70	2.52	0.07

4 Conclusion

Structural and microstructural evolution and thus changes of magnetic properties of MA and oxidized Fe-Ni and Fe-Ni-Cr powders have been investigated. The results show the formation of two ferromagnetic solid solutions bcc and fcc in mechanically alloyed samples. After oxidation, Rietveld refinement reveals the formation of three types of oxides on the surface of particles: AFM NiO and α -Fe₂O₃ phases and about 50 % of ferrimagnetic inverse spinel NiFe₂O₄ phase. It has been found that the magnetic coupling between FM cores and AFM shell leads to the decrease of Ms and the increase of Hc.

References

- Suryanarayana, C.: *Int. Mater. Rev.* **40**, 41 (1995)
- Lu, K.: *Mater. Sci. Eng. R* **16**, 161 (1996)
- McHenry, M.E., Villard, M.A., Laughlin, D.E.: *Prog. Mater. Sci.* **44**, 291 (1999)
- Baldokhin, Y.V., Kolotykin, P.Y., Petrov, Y.I., Shafranovsky, E.A.: *Phys. Lett. A* **189**, 137 (1994)
- Yu, R.H., Ren, L., Basu, S., Unruh, K.M., Parvizi-Majidi, A., Xiao, J.Q.: *J. Appl. Phys.* **87**, 5840 (1999)
- Djekoun, A., Bouzabata, B., Alleg, S., Grenèche, J.M., Otmani, A.: *Ann. Chim. Sci. Mater.* **23**, 557 (1998)
- Sunol, J.J., Gonzalez, A., Escoda, L.: *J. Mater. Sci.* **39**, 5147 (2004)
- Li, X.G., Chiba, A., Takahashi, S.: *J. Magn. Magn. Mater.* **170**, 339 (1997)
- Suryanarayana, C.: *Bull. Mater. Sci.* **17**, 307 (1994)
- Suryanarayana, C.: *Prog. Mater. Sci.* **46**, 1 (2001)
- Tcheryntsev, V.V., Kaloshkin, S.D., Tomilin, I.A., Shelekov, E.V., Baldokhin, Y.V.: *Nanostruct. Mater.* **12**, 139 (1999)
- He, Q., Liu, T., Xie, J.L.: *Key Eng. Mater.* **437**, 531–532 (2012)
- Oberg, E. *Machinery's Handbook*, 25th edn., p. 411. Industrial Press Inc, New York (1996)
- Harris, T.E., Whitney, G.M., Croll, I.M.: *J. Electrochem. Soc.* **142**, 1031 (1995)
- Andricacos, P.C., Robertson, N.: *IBM J. Res. Dev.* **42**, 671 (1998)
- Yen, Y., Su, J., Huang, D.: *J. Alloys Compd.* **457**, 270 (2008)
- Enayati, M.H., Bafandeh, M.R.: *J. Alloys Compd.* **454**, 228 (2008)
- Shuchua, G., Yuping, D., Peng, D., Song, W., Guoping, Q., Yuzhe, L.: *J. Electron. Mater.* **44**, 7 (2015)
- Rietveld, H.M.: *Acta Crystallogr.* **22**, 151 (1967)
- Rietveld, H.M.: *J. Appl. Cryst.* **2**, 65 (1969)
- Young, R.A. (ed.): *The Rietveld Method*. Oxford University Press/IUCr (1996)
- Porter, D.A.: *Phase Transformation in Metals and Alloys*. Chapman & Hall, London (1996)
- Gheisari, K., Javadpour, S., Oh, J.T., Ghaffari, M.: *J. Alloys Compd.* **472**, 416 (2009)
- Khurt, C., Schultz, L.: *J. Appl. Phys.* **73**, 1975 (1993)
- Yermakov, A.Y., Yurchikov, Y.Y., Barinow, V.A.: *Phys. Met. Metallogr.* **52**, 50 (1981)
- Hadef, F., Otmani, A., Djekoun, A., Grenèche, J.M.: *J. Magn. Magn. Mater.* **343**, 214 (2013)
- Valderruten, J.F., PérezAlcazar, G.A., Grenèche, J.M.: *Physica B* **384**, 316 (2006)
- Smit, J., Wijn, H.P.J.: *Ferrites-Physical Properties of Ferrimagnetic Oxides in Relation to their Technical Applications*. Wiley, The Netherlands (1959)
- Chinnasamy, C.N., Narayanasamy, A., Ponpandian, N., Chattopadhyay, K., Guerault, H., Grenèche, J.M.: *J. Phys. Condens. Matter* **12**, 7795 (2000)
- Gale, W.F., Totemeier, T.C. *Smithells Metal Reference Book*, 8th edn. Elsevier, Amsterdam (2004)
- Bid, S., Sahu, P., Pradhan, S.K.: *Physica E* **39**, 175 (2007)
- Valderruten, J.F., Pérez Alcázar, G.A., Grenèche, J.M.: *J. Phys. Condens. Matter* **20**, 485204 (2008)
- Palacio, D.C., Valderruten, J.F., Zamora, L.E., Pérez Alcázar, G.A., Tabares, J.A.: *Hyperfine Interact.* **195**, 241 (2010)
- Men'shikov, A.Z., Sidorov, S.K., Teplykh, A.E.: *Fis. Metallov I Metallovedenie.* **45**, 949 (1978)
- Majumdar, A.K., Blanckenhagen, P.V.: *Phys. Rev. B* **29**, 4079 (1984)
- Krifa, M., Mhadhbi, M., Escoda, L., Saurina, J., Suñol, J.J., Llorca-Isern, N., Artieda-Guzmán, C., Khitouni, M.: *Powder Technol.* **246**, 117 (2013)
- Shokrollahi, H.: *Mater. Des.* **30**, 3374 (2009)
- Vitta, S., Khuntia, A., Ravikumar, G., Bahadur, D.: *J. Magn. Magn. Mater.* **320**, 182 (2008)
- Kaloshkin, S.D., Tcheryntsev, V.V., Baldokhin, Y.V., Tomilin, I.A., Shelekhov, E.V.: *J. Non-Cryst. Solids* **287**, 329 (2001)
- Müller, J.B., Hesse, J.: *Phys. B: Condens. Matter* **54**, 35 (1984)
- Hamzaoui, R., Elkedim, O., Fenineche, N., Gaffet, E., Craven, J.: *J. Mater. Sci. Eng. A* **360**, 299 (2003)
- Yousefzadeh, M., Zandrahimi, M.: *Proceedings of the 4th International Conference on Nanostructures (ICNS4)*. Kish Island, I.R. Iran (2012)
- Respaud, M., Broto, J.M., Rakoto, H., Thoma, A.R., Fert, L., Verelst, B., Barbara, M., Snoeck, E., Lecante, P., Osuna, A., Mosset, J., Ould Ely, T., Amiens, C., Chaudret, B.: *Phys. Rev. B* **57**, 2925 (1998)
- Set, T., Akinaga, H., Koga, K., Orii, T., Hirasawa, M.: *J. Phys. Chem. B Lett.* **109**, 13403 (2005)
- Goldman, A.: *Modern Ferrites Technology* **2**, 32 (2006)